Article

Coprime Transformed Nested Array with Enhanced DOFs and Reduced Mutual Coupling Based on the Difference and Sum Coarray

Junchi Ma [1], **Shunan Zhong** [1], **Zhe Peng** [1], **Wei Gao** [1,*], **Weijiang Wang** [1,2] **and Xiaohua Wang** [1]

[1] School of Integrated Circuits and Electronics, Beijing Institute of Technology, Beijing 100081, China; bitmajunchi@163.com (J.M.); zhongsabit@163.com (S.Z.); 3120185386@bit.edu.cn (Z.P.); wangweijiangbit@163.com (W.W.); wangxiaohuabit@163.com (X.W.)
[2] Beijing Institute of Technology Chongqing Center for Microelectronics and Microsystems, Chongqing 401332, China
[*] Correspondence: titigw@bit.edu.cn; Tel.: +86-010-6891-8356

Abstract: Recently, the concept of the difference and sum coarray has attracted increasing interest in the direction of the arrival estimation field because it can generate enhanced degrees of freedom. In this paper, we propose an improved transformed nested array design strategy by relaxing the constraints on the dense subarray of the transformed nested array. Then, three conditions are given for the array design to ensure the continuity of the difference and sum coarray. Based on the strategy, we develop a novel nested configuration named coprime transformed nested array (CTNA) whose dense subarray is a coprime structure, and the closed-form expressions for the sensor positions and the range of consecutive coarray are derived. CTNA can increase the number of degrees of freedom (DOFs) compared to the existing nested arrays, while the mutual coupling effect can be maintained at the same low level as the coprime arrays, which indicates that CTNA has the merits of both nested array and coprime array. Numerical simulations are performed to verify the superiority of the proposed array configuration in terms of the number of DOFs, mutual coupling and direction of arrival (DOA) estimation accuracy.

Keywords: degree of freedom; difference and sum coarray; DOA estimation; mutual coupling

1. Introduction

Direction of arrival (DOA) estimation is an important topic in array signal processing and has been extensively applied in various fields, such as radar, sonar, navigation and wireless communication [1–8]. Traditional subspace-based DOA estimation methods, such as MUSIC [9] and ESPRIT [10], can identify at most $R - 1$ sources with an R-sensor uniform linear array (ULA). Thus, more sensors are needed in ULA for identifying more sources, resulting in higher hardware cost and computational complexity.

In order to identify more sources than the number of sensors, sparse arrays, such as minimum redundancy array (MRA) [11] and minimum hole array (MHA) [12], are proposed. By vectorizing the covariance matrix of the received signal, the difference coarray of these sparse arrays can provide $O(R^2)$ degrees of freedom (DOFs) with only R sensors. However, MRA and MHA do not have closed-form expressions for the array geometry and the number of achievable DOFs, which limits their application in practice.

The recently proposed nested array and coprime array have received considerable interest since they can overcome the shortcomings of MRA and MHA. Prototype nested array (NA) [13] consists of a dense ULA and a sparse ULA, which can provide a large number of DOFs. Due to the closely arranged sensors in the dense ULA, NA suffers from a severe mutual coupling effect. To tackle the problem, super nested array (SNA) [14,15] is developed by redistributing the sensors of the dense ULA to reduce the mutual coupling.

To increase the number of DOFs and reduce mutual coupling at the same time, augmented nested array (ANA) [16] and extended nested array (ENA) [17] are proposed by separating the dense ULA into two sections, then rearranging one section to the right of the sparse ULA. On the other hand, prototype coprime array (CA) [18–20] is composed of an *M*-element ULA with inter-element spacing *N* units and an *N*-element ULA with inter-element spacing *M* units, where *M* and *N* are coprime integers. Since many holes exist in the difference coarray of CA, the accuracy of the DOA estimation will deteriorate when spatial smoothing-based algorithms [21,22] are used. Conventional coprime array (CCA) developed in [23] can obtain more consecutive virtual elements by increasing the number of sensors in one subarray from *M* to 2*M*. A thinned coprime array (TCA) [24] is constructed by removing $\lceil M/2 \rceil$ redundant sensors from CCA, and the difference coarray of TCA is the same as that of CCA. Therefore, TCA can further increase the number of available DOFs and reduce the mutual coupling effect. Padded coprime array (PCA) [25] and rearranged coprime array (RCA) [26] introduce a subarray to fill the holes in the difference coarray so more DOFs can be achieved.

However, the aforementioned work only considers the difference coarray. If the difference coarray and the sum coarray can be used jointly, the DOA estimation accuracy can be further improved. In [27], the authors propose a vectorized conjugate augmented MUSIC (VCAM) algorithm. This algorithm can construct the difference and sum coarray (diff-sum coarray) by using both the spatial information and the temporal information of the received signal. Some novel sparse arrays are developed based on the diff-sum coarray. To increase the number of consecutive virtual elements, the diff-sum nested array (DsNA) [28] is designed by rearranging half of the sensors in the dense subarray to the sparse subarray. In [29], the authors propose a transformed nested array (TNA) by exchanging the positions of the two subarrays of prototype NA, which can decrease the overlapping virtual elements between the difference and the sum coarray. The extended transformed nested array (ETNA) proposed in [30] can further reduce the redundancy by redesigning the dense subarray of TNA. By using $\lceil M/2 \rceil$ unimportant sensors of CCA to construct a supplementary subarray, the supplementary coprime array (SCA) [31] can expand the consecutive diff-sum coarray range and reduce mutual coupling at the same time.

Generally speaking, the existing nested arrays can provide more DOFs but suffer from a severe mutual coupling effect. In contrast, coprime arrays are not sensitive to mutual coupling, but provide fewer DOFs than nested arrays. In this paper, we focus on designing a sparse array with the merits of nested array and coprime array based on the diff-sum coarray. Firstly, we propose an improved transformed nested array design strategy, which relaxes the constraints on the dense subarray of TNA and provides three continuity conditions to ensure that the corresponding diff-sum coarray has a long consecutive segment. Based on this strategy, we design a novel nested configuration named coprime transformed nested array (CTNA), whose dense subarray is a coprime array. The coprime array is more sparse than the existing dense subarrays since the number of sensor pairs with small spacing is independent of the array size, which significantly reduces the mutual coupling effect. Meanwhile, CTNA can provide more DOFs than the existing sparse arrays. Extensive simulations are performed to evaluate the effectiveness of the proposed array configuration, according to the number of DOFs, mutual coupling and DOA estimation accuracy.

The rest of the paper is organized as follows. Section 2 introduces the signal model and the VCAM algorithm. Section 3 provides the improved transformed nested array design strategy and develops the CTNA array configuration. The properties of CTNA, including the number of available DOFs and the weight function values, are presented in Section 4. Numerous simulation results are shown in Section 5. Section 6 concludes this paper.

Notations: In this paper, we use $(\cdot)^*$, $(\cdot)^T$, $(\cdot)^H$ to represent complex conjugation, transpose and conjugate transpose, respectively. $E[\cdot]$ and $vec(\cdot)$ denote statistical expectation and vectorization, respectively. The symbol $\otimes$ is a Kronecker product and $\odot$ is a Khatri–Rao product. $\boldsymbol{I}_n$ is the $n \times n$ identity matrix. $\mathbb{A} - \mathbb{B} = \{a - b | a \in \mathbb{A}, b \in \mathbb{B}\}$ and

$\mathbb{A} + \mathbb{B} = \{a + b | a \in \mathbb{A}, b \in \mathbb{B}\}$ respectively represent the difference set and the sum set of $\mathbb{A}$ and $\mathbb{B}$.

2. Preliminaries

2.1. Data Model

Assume K far-field narrowband uncorrelated sources from direction $\{\theta_1, \theta_2, ..., \theta_K\}$ impinging on an R-element linear sparse array whose sensor positions are given by $\mathbb{L} = \{l_1, l_2, ..., l_R\}d$, where d represents the unit inter-element spacing and is set to half the wavelength of the signals. According to [27], the k-th signal can be expressed as $s_k(t) = A_k e^{j(\omega_c + \omega_k)t}$, where A_k is complex amplitude, and ω_c and ω_k denote the carrier frequency and baseband frequency, respectively. Without loss of generality, we assume that the carrier frequency is much larger than the baseband frequency, i.e., $\omega_c \gg \omega_k$, and different signals have different baseband frequencies, i.e., $\omega_k \neq \omega_m$ if $k \neq m$. Then, the received signal is demodulated to the intermediate frequency, the k-th signal becomes $s_k(t) = A_k e^{j\omega_k t}$, and the received data can be modeled as

$$x(t) = \sum_{k=1}^{K} a(\theta_k)s_k(t) + n(t) = As(t) + n(t), \tag{1}$$

where $a(\theta_k) = [e^{j2\pi l_1 d \sin(\theta_k)/\lambda}, e^{j2\pi l_2 d \sin(\theta_k)/\lambda}, ..., e^{j2\pi l_R d \sin(\theta_k)/\lambda}]^T$ is a steering vector corresponding to the kth signal with λ being the carrier wavelength; $A = [a(\theta_1), a(\theta_2), ..., a(\theta_K)]$ represents the manifold matrix; $s(t) = [s_1(t), s_2(t), ..., s_K(t)]^T$ is the source vector; and $n(t) = [n_1(t), n_2(t), ..., n_R(t)]^T$ denotes the white Gaussian noise vector with zero mean and variance σ_n^2.

2.2. VCAM Algorithm

We use the VCAM algorithm [27] to construct the diff-sum coarray in this paper. Two data vectors $[x_1(1), x_1(2), ..., x_1(T)]$ and $[x_r(1 + \tau), x_r(2 + \tau), ..., x_r(T + \tau)]$ can be generated by collecting T snapshots from the first sensor output $x_1(t)$ and the r-th $(1 \leq r \leq R)$ sensor output $x_r(t)$. Then, the time average function of $x_1^*(t)$ and $x_r(t + \tau)$ can be calculated as

$$R_{x_1^* x_r}(\tau) = \frac{1}{T} \sum_{t=1}^{T} x_1^*(t)x_r(t + \tau)$$
$$= \sum_{k=1}^{K} \sum_{m=1}^{K} a_1^*(\theta_k)a_r(\theta_m)A_k^* A_m e^{j\omega_m \tau}\left(\frac{1}{T}\sum_{t=1}^{T} e^{j(\omega_m - \omega_k)t}\right) + R_{n_1^* n_r}(\tau), \tag{2}$$

where $R_{n_1^* n_r}(\tau) = \frac{1}{T}\sum_{t=1}^{T} n_1^*(t)n_r(t + \tau) = 0$ when $\tau \neq 0$. Since $\frac{1}{T}\sum_{t=1}^{T} e^{j(\omega_k - \omega_m)t}$ is approximately equal to 0 if $\omega_k \neq \omega_m$ and T is sufficiently large, (2) can be simplified as

$$R_{x_1^* x_r}(\tau) = \sum_{k=1}^{K} e^{j2\pi l_r d \sin(\theta_k)/\lambda} R_{s_k^* s_k}(\tau), \tag{3}$$

where $R_{s_k^* s_k}(\tau) = |A_k|^2 e^{j\omega_k \tau}$. As $R_{s_k^* s_k}(\tau)$ is similar to the signal $s_k(t) = A_k e^{j\omega_k t}$, $R_{s_k^* s_k}(\tau)$ can be regarded as an equivalent signal coming from the direction θ_k.

Combining $R_{x_1^* x_r}(\tau)$ for each $r = 1, 2, ..., R$, the following vector can be generated as

$$v_x(\tau) = [R_{x_1^* x_1}(\tau), R_{x_1^* x_2}(\tau), ..., R_{x_1^* x_R}(\tau)]^T = Av_s(\tau), \tag{4}$$

where $v_s(\tau) = [R_{s_1^* s_1}(\tau), R_{s_2^* s_2}(\tau), ..., R_{s_K^* s_K}(\tau)]^T$. Similarly,

$$v_x^*(-\tau) = [R_{x_1^* x_1}^*(-\tau), R_{x_1^* x_2}^*(-\tau), ..., R_{x_1^* x_R}^*(-\tau)]^T = A^* v_s^*(-\tau) = A^* v_s(\tau). \tag{5}$$

The last equation holds since $R_{s_k^* s_k}(\tau) = R_{s_k^* s_k}^*(-\tau)$ for $k = 1, 2, ..., K$. Combining $v_x^*(-\tau)$ and $v_x(\tau)$, augmented vector $v(\tau)$ can be obtained as

$$v(\tau) = \begin{bmatrix} v_x^*(-\tau) \\ v_x(\tau) \end{bmatrix} = \begin{bmatrix} A^* \\ A \end{bmatrix} v_s(\tau) = \bar{A} v_s(\tau), \tag{6}$$

where $\bar{A} = [A^T, A^H]^H = [\bar{a}(\theta_1), \bar{a}(\theta_2)..., \bar{a}(\theta_K)]$, $\bar{a}(\theta_k) = [a(\theta_k)^T, a(\theta_k)^H]^H$. By gathering augmented vector $v(\tau)$ at moment $\tau = \tau_s, 2\tau_s, ..., P\tau_s$, the pseudo data matrix V can be constructed as follows:

$$V = [v(\tau_s), v(2\tau_s), ..., v(P\tau_s)] = \bar{A}[v_s(\tau_s), v_s(2\tau_s), ..., v_s(P\tau_s)] = \bar{A}DE, \tag{7}$$

where τ_s and P are defined as the pseudo sampling period and the number of pseudo snapshots, respectively; $D = \mathrm{diag}\{|A_1|^2, |A_2|^2, ..., |A_Q|^2\}$; $E = [v_s'(\tau_s)v_s'(2\tau_s), ..., v_s'(P\tau_s)]$ with $v_s'(p\tau_s) = [e^{j\omega_1 p\tau_s}, e^{j\omega_2 p\tau_s}, ..., e^{j\omega_K p\tau_s}]^T$, $p = 1, 2, ..., P$.

The covariance matrix of augmented vector $v(\tau)$ can be obtained as

$$R_v = \frac{1}{P}VV^H = \bar{A}D(\frac{1}{P}EE^H)D^H\bar{A}^H, \tag{8}$$

where the (k, m)-th element of $\frac{1}{P}EE^H$ is $\frac{1}{P}\sum_{p=1}^{P} e^{j(\omega_k - \omega_m)p\tau_s}$. If P is sufficiently large and $k \neq m$, this element is approximately equal to 0. Therefore, $\frac{1}{P}EE^H$ can be regarded as a $K \times K$ identity matrix, and covariance matrix R_v can be simplified as

$$R_v = \bar{A}R_s\bar{A}^H, \tag{9}$$

where $R_s = \mathrm{diag}\{|A_1|^4, |A_2|^4, ..., |A_Q|^4\}$. Then, R_v can be vectorized as

$$z = \mathrm{vec}\{R_v\} = (\bar{A}^* \odot \bar{A})p, \tag{10}$$

where $p = [|A_1|^4, |A_2|^4, ..., |A_Q|^4]^T$, the k-th column of $\bar{A}^* \odot \bar{A}$ is

$$\bar{a}^*(\theta_k) \otimes \bar{a}(\theta_k) = \begin{bmatrix} a^*(\theta_k) \\ a(\theta_k) \end{bmatrix}^* \otimes \begin{bmatrix} a^*(\theta_k) \\ a(\theta_k) \end{bmatrix} = J \begin{bmatrix} a(\theta_k) \otimes a^*(\theta_k) \\ a(\theta_k) \otimes a(\theta_k) \\ a^*(\theta_k) \otimes a^*(\theta_k) \\ a^*(\theta_k) \otimes a(\theta_k) \end{bmatrix}, \tag{11}$$

where J is a $4R^2 \times 4R^2$ permutation matrix defined in [30].

It can be seen from (11) that $\bar{a}^*(\theta_k) \otimes \bar{a}(\theta_k)$ consists of four parts, where the first and fourth parts correspond to difference coarray $\mathbb{L}_D = \mathbb{L} - \mathbb{L} = \{(l_1 - l_2)d | l_1, l_2 \in \mathbb{L}\}$, the second and third parts respectively correspond to positive sum coarray $\mathbb{L}_S^+ = \mathbb{L} + \mathbb{L} = \{(l_1 + l_2)d | l_1, l_2 \in \mathbb{L}\}$ and negative sum coarray $\mathbb{L}_S^- = -\mathbb{L} - \mathbb{L} = \{-(l_1 + l_2)d | l_1, l_2 \in \mathbb{L}\}$. As a result, $\bar{a}^*(\theta_k) \otimes \bar{a}(\theta_k)$ is the equivalent steering vector of the diff-sum coarray, and z is the equivalent received signal of the diff-sum coarray. Assume that the diff-sum coarray is continuous in the range $[-l_u d, l_u d]$. After eliminating the repeated and discrete elements of z, we can obtain

$$\hat{z} = \hat{A}p, \tag{12}$$

where $\hat{A}$ is the array manifold matrix of consecutive diff-sum coarray elements. After that, we use the spatial smoothing MUSIC (SS-MUSIC) [21] algorithm to perform the DOA estimation.

The main computational load of the VCAM algorithm includes the construction of pseudo data matrix V, calculation of covariance matrix R_v, spatial smoothing operation, eigenvalue decomposition and spatial spectrum search. The computational complexity of the above steps is $O(2RTP)$, $O(4PR^2)$, $O((l_u + 1)^3)$, $O(\frac{4}{3}(l_u + 1)^3)$ and $O(\frac{\pi}{\Delta\theta}(l_u + 1)^2)$, respectively, where l_u represents the maximum one-side aperture of the consecutive diff-sum coarray, and $\Delta\theta$ is the search interval of DOA. As a result, the total computational complexity of the VCAM algorithm is $O(2RTP + 4PR^2 + (l_u + 1)^3 + \frac{4}{3}(l_u + 1)^3 + \frac{\pi}{\Delta\theta}(l_u + 1)^2)$.

2.3. Mutual Coupling

In practice, the mutual coupling effect between two sensors with small spacing is inevitable. For a linear array, the mutual coupling matrix C can be modeled as a B-banded Toeplitz matrix [14,32–34], whose (m, n)-th element is expressed as

$$[C]_{m,n} = \begin{cases} c_{|l_m - l_n|}, & \text{if } |l_m - l_n| \leq B \\ 0, & \text{otherwise} \end{cases}, \tag{13}$$

where $l_m, l_n \in \mathbb{L}$. The magnitudes of coupling coefficients are inversely proportional to sensor spacing and satisfy $c_0 = 1 > |c_1| > |c_2| > ... > |c_B| > 0$. In this paper, the coupling coefficients are set to $c_0 = 1$, $c_1 = |c_1|e^{j\pi/3}$ and $c_l = c_1 e^{-j(l-1)\pi/8}/l, 2 \leq l \leq B$. Therefore, the received data model in (1) can be rewritten as

$$x(t) = CAs(t) + n(t). \tag{14}$$

To evaluate the mutual coupling effect conveniently, we introduce the weight function $\omega(m)$ defined as follows.

Definition 1. *The weight function $\omega(m)$ of a physical array $\mathbb{L}$ denotes the number of sensor pairs with spacing md, i.e.,*

$$w(m) = Card(\mathbb{W}(m)), \tag{15}$$

where

$$\mathbb{W}(m) = \{(l_1, l_2) \in \mathbb{L}^2 | l_1 - l_2 = md\}, \tag{16}$$

Card(·) denotes the cardinality of a set.

We should focus on the weight functions corresponding to small spacing since they have a significant impact on the mutual coupling effect. In addition, the definition of coupling leakage is also given to quantify the mutual coupling effect.

Definition 2. *The coupling leakage E can be defined as*

$$E = \frac{\|C - diag(C)\|_F}{\|C\|_F}, \tag{17}$$

where $\|\cdot\|_F$ denotes the Frobenius norm and $diag(C)$ is a diagonal matrix constructed by the diagonal elements of C.

$\|C\|_F$ is the total energy of the mutual coupling matrix, and $\|C - \text{diag}(C)\|_F$ represents the energy of off-diagonal elements. Therefore, the coupling leakage E is the ratio of the leakage energy to the total energy. The smaller E is, the lesser the mutual coupling.

3. Coprime Transformed Nested Array

3.1. Improved Transformed Nested Array Design Strategy

For prototype NA, the difference coarray is a subarray of the sum coarray [28], which means that there are many redundant virtual elements in its diff-sum coarray. To solve this problem, the transformed nested array (TNA) is proposed in [29], whose sensor position set is given by

$$\mathbb{L}_{\text{TNA}} = \mathbb{L}_s \cup \mathbb{L}_d, \tag{18}$$

where

$$\mathbb{L}_s = \{n_1(N_2 + 1) \mid 0 \leq n_1 \leq N_1 - 1\},$$
$$\mathbb{L}_d = \{(N_1 - 1)(N_2 + 1) + n_2 \mid 0 \leq n_2 \leq N_2\}.$$

Here, all the positions are normalized by d for convenience. It is clear that the sparse subarray $\mathbb{L}_s$ is an N_1-element ULA with inter-element spacing $(N_2 + 1)$, and the dense subarray $\mathbb{L}_d$ is an $(N_2 + 1)$-element ULA with unit inter-element spacing.

Different from prototype NA, the dense subarray $\mathbb{L}_d$ is on the right side of the sparse subarray $\mathbb{L}_s$ in TNA. By swapping the positions of the two subarrays, the corresponding difference coarray remains unchanged, and the positive and the negative sum coarray are shifted to both sides along with the axis, respectively. Thus, the redundancy between the difference coarray and the sum coarray can be significantly reduced. The diff-sum coarray of TNA can provide more DOFs than that of prototype NA. An example of TNA with parameters $N_1 = 4$, $N_2 = 6$ is illustrated in Figure 1. Due to the symmetry of the diff-sum coarray, only the non-negative virtual elements are considered. It can be seen that the difference coarray and the sum coarray are continuous in the range $[0, 27]$ and $[21, 54]$, respectively. Thus, the diff-sum coarray possesses all the virtual elements in the range $[0, 54]$. There are only 10 overlapping elements between the difference coarray and the sum coarray.

The difference coarray of TNA consists of the self-difference sets $\mathbb{L}_d - \mathbb{L}_d$, $\mathbb{L}_s - \mathbb{L}_s$ and the cross-difference set $\mathbb{L}_d - \mathbb{L}_s$, where $\mathbb{L}_s - \mathbb{L}_s$ is a subset of $\mathbb{L}_d - \mathbb{L}_s$. The sum coarray of TNA consists of the self-sum sets $\mathbb{L}_d + \mathbb{L}_d$, $\mathbb{L}_s + \mathbb{L}_s$ and the cross-sum set $\mathbb{L}_d + \mathbb{L}_s$, where $\mathbb{L}_s + \mathbb{L}_s$ is a subset of $(\mathbb{L}_d - \mathbb{L}_s) \cup (\mathbb{L}_d + \mathbb{L}_s)$. It is noteworthy that $\mathbb{L}_d - \mathbb{L}_d$ and $\mathbb{L}_d + \mathbb{L}_d$ make little contribution to the diff-sum coarray; most of the virtual elements in the diff-sum coarray are generated by cross sets $\mathbb{L}_d - \mathbb{L}_s$ and $\mathbb{L}_d + \mathbb{L}_s$. As shown in Figure 1b,c, $\mathbb{L}_d - \mathbb{L}_d$ is completely contained in $\mathbb{L}_d - \mathbb{L}_s$, and half of the elements in $\mathbb{L}_d + \mathbb{L}_d$ overlap with $\mathbb{L}_d + \mathbb{L}_s$. In addition, TNA suffers from a severe mutual coupling effect due to the closely distributed sensors in the dense subarray. So we hope to find a more sparse structure instead of the ULA as the dense subarray of TNA to increase the number of DOFs and reduce the mutual coupling effect. First, the novel dense subarray must ensure that the cross-difference set $\mathbb{L}_d - \mathbb{L}_s$ and the cross-sum set $\mathbb{L}_d + \mathbb{L}_s$ can generate a long continuous segment in the diff-sum coarray.
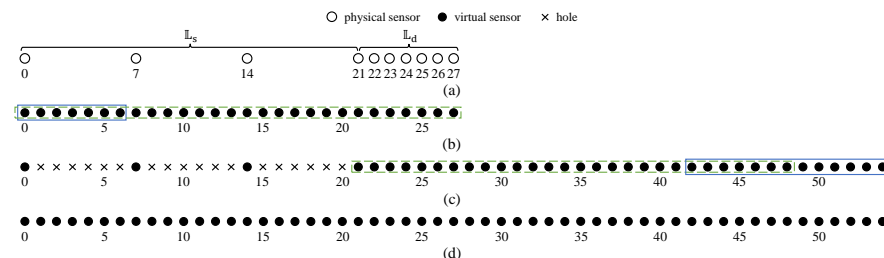

Figure 1. An example of transformed nested array and its coarrays, where $N_1 = 4$, $N_2 = 6$. (**a**) Physical array. (**b**) Difference coarray. Green dashed box and blue solid box respectively represent the elements in $\mathbb{L}_d - \mathbb{L}_s$ and $\mathbb{L}_d - \mathbb{L}_d$. (**c**) Sum coarray. Green dashed box and blue solid box respectively represent the elements in $\mathbb{L}_d + \mathbb{L}_s$ and $\mathbb{L}_d + \mathbb{L}_d$. (**d**) Diff-sum coarray.

For the original dense subarray $\mathbb{L}_d = \{(N_1 - 1)(N_2 + 1) + n_2 \mid 0 \leq n_2 \leq N_2\}$, any element $l_i \in \mathbb{L}_d, i = 1, 2, ..., N_2 + 1$ can be rewritten as $l_i = a_i(N_2 + 1) + b_i$, where a_i and b_i are quotient and remainder of $l_i / (N_2 + 1)$, $a_i = N_1 - 1$, $b_i \in [0, N_2]$. Therefore, the dense subarray of TNA satisfies two constraints. The first one is the remainder constraint, that is, $\mathcal{R}[\mathbb{L}_d]_{N_2+1} = \{b_1, b_2, ..., b_{N_2+1}\} = [0, N_2]$, where $\mathcal{R}[\mathbb{A}]_b = \{a \bmod b \mid a \in \mathbb{A}\}$ represents the remainder set of $\mathbb{A}$ and mod is the modulo operation. The second one is the quotient constraint, that is, $a_1 = a_2 = \cdots = a_{N_2+1} = N_1 - 1$. We find that if $\mathbb{L}_d$ only satisfies the remainder constraint but not the quotient constraint, $\mathbb{L}_d$ will be more sparse, and the cross sets $(\mathbb{L}_d - \mathbb{L}_s) \cup (\mathbb{L}_d + \mathbb{L}_s)$ can still produce a large number of consecutive virtual elements in the diff-sum corray. To illustrate this situation, we give an example in Figure 2. It can be seen from Figure 2a that the dense subarray is located at $\mathbb{L}_d = \{21, 22, 25, 26, 27, 30, 31\}$, and satisfies the remainder constraint $\mathcal{R}[\mathbb{L}_d]_7 = [0, 6]$. The corresponding cross-difference set $\mathbb{L}_d - \mathbb{L}_s$ and cross-sum set $\mathbb{L}_d + \mathbb{L}_s$ contain all the consecutive virtual elements in the range

[4, 48]. Based on this observation, we summarize the properties of $(\mathbb{L}_d - \mathbb{L}_s) \cup (\mathbb{L}_d + \mathbb{L}_s)$ as follows.
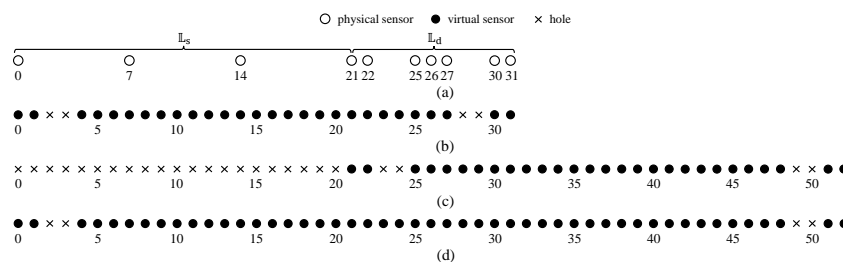

Figure 2. An example of transformed nested array that satisfies the remainder constraint, where $N_1 = 4$, $N_2 = 6$. (**a**) Physical array. (**b**) Cross-difference set $\mathbb{L}_d - \mathbb{L}_s$. (**c**) Cross-sum set $\mathbb{L}_d + \mathbb{L}_s$. (**d**) $(\mathbb{L}_d - \mathbb{L}_s) \cup (\mathbb{L}_d + \mathbb{L}_s)$.

Theorem 1. *Consider a nested-like array configuration whose sparse subarray is an N_1-element ULA located at $\mathbb{L}_s = \{n_1(N_2 + 1) \mid 0 \le n_1 \le N_1 - 1\}$, dense subarray $\mathbb{L}_d$ has $N_2 + 1$ elements and satisfies the remainder constraint $\mathcal{R}[\mathbb{L}_d]_{N_2+1} = [0, N_2]$, $\mathbb{L}_s$ is on the left side of $\mathbb{L}_d$. Without loss of generality, we assume that quotient a_i of element $l_i \in \mathbb{L}_d$ satisfying $a_i \in [N_1 - 1, N_1 - 1 + a_{max}]$ for $i = 1, 2, ..., N_2 + 1$, where a_{max} is the maximum value of $a_i - N_1 + 1$. Then, the cross-difference set $\mathbb{L}_d - \mathbb{L}_s$ and the cross-sum set $\mathbb{L}_d + \mathbb{L}_s$ have the following properties:*

(a) *$(\mathbb{L}_d - \mathbb{L}_s) \cup (\mathbb{L}_d + \mathbb{L}_s)$ contains all the virtual elements in the range $[a_{max}(N_2 + 1), (2N_1 - 1)(N_2 + 1) - 1]$.*

(b) *In the range $[c(N_2 + 1), (c + 1)(N_2 + 1) - 1], 0 \le c \le a_{max} - 1$, the position $l_i - (a_i - c)(N_2 + 1)$ is a hole if $N_1 \le a_i - c \le N_1 - 1 + a_{max}$.*

(c) *In the range $[c(N_2 + 1), (c + 1)(N_2 + 1) - 1], 2N_1 - 1 \le c \le 2N_1 - 2 + a_{max}$, the position $l_i + (c - a_i)(N_2 + 1)$ is a hole if $N_1 \le c - a_i \le N_1 - 1 + a_{max}$.*

Proof. First, we divide the range $[0, (2N_1 - 1 + a_{max})(N_2 + 1) - 1]$ into several small ranges $[c(N_2 + 1), (c + 1)(N_2 + 1) - 1]$, where $0 \le c \le 2N_1 - 2 + a_{max}$. The range $[c(N_2 + 1), (c + 1)(N_2 - 1) - 1]$ can be rewritten as $c(N_2 + 1) + \{b_1, b_2, ..., b_{N_2+1}\}$ since $\mathbb{L}_d$ satisfies the remainder constraint $\mathcal{R}[\mathbb{L}_d]_{N_2+1} = \{b_1, b_2, ..., b_{N_2+1}\} = [0, N_2]$. Therefore, any element $c(N_2 + 1) + b_i$ in the range $[c(N_2 + 1), (c + 1)(N_2 + 1) - 1]$ can be expressed as $l_i - (a_i - c)(N_2 + 1)$ since

$$l_i - (a_i - c)(N_2 + 1) = a_i(N_2 + 1) + b_i - (a_i - c)(N_2 + 1) = c(N_2 + 1) + b_i. \tag{19}$$

Based on the value of c, we can divide the virtual element $l_i - (a_i - c)(N_2 + 1)$ into three cases:

(a) $c \in [a_{max}, 2N_1 - 2], a_i - c \in [-N_1 + 1, N_1 - 1]$. If $a_i - c \in [0, N_1 - 1]$, then $(a_i - c)(N_2 + 1) \in \mathbb{L}_s$, this virtual element can be generated by the cross-difference set $\mathbb{L}_d - \mathbb{L}_s$. If $a_i - c \in [-N_1 + 1, 0]$, then $(c - a_i)(N_2 + 1) \in \mathbb{L}_s$, this virtual element can be generated by the cross-sum set $\mathbb{L}_d + \mathbb{L}_s$. Therefore, $(\mathbb{L}_d - \mathbb{L}_s) \cup (\mathbb{L}_d + \mathbb{L}_s)$ is continuous in the range $[a_{max}(N_2 + 1), (2N_1 - 1)(N_2 + 1) - 1]$.

(b) $c \in [0, a_{max} - 1], a_i - c \in [N_1 - a_{max}, N_1 - 1 + a_{max}]$. If $a_i - c \in [N_1 - a_{max}, N_1 - 1]$, then $(a_i - c)(N_2 + 1) \in \mathbb{L}_s$, this virtual element can be generated by $\mathbb{L}_d - \mathbb{L}_s$. If $a_i - c \in [N_1, N_1 - 1 + a_{max}]$, then $(a_i - c)(N_2 + 1) \notin \mathbb{L}_s$, this virtual element can not be generated by $(\mathbb{L}_d - \mathbb{L}_s) \cup (\mathbb{L}_d + \mathbb{L}_s)$. As a result, the position $l_i - (a_i - c)(N_2 + 1)$ with $a_i - c \in [N_1, N_1 - 1 + a_{max}]$ is a hole.

(c) $c \in [2N_1 - 1, 2N_1 - 2 + a_{max}], c - a_i \in [N_1 - a_{max}, N_1 - 1 + a_{max}]$. If $c - a_i \in [N_1 - a_{max}, N_1 - 1]$, then $(c - a_i)(N_2 + 1) \in \mathbb{L}_s$, this virtual element can be generated by $\mathbb{L}_d + \mathbb{L}_s$. If $c - a_i \in [N_1, N_1 - 1 + a_{max}]$, then $(c - a_i)(N_2 + 1) \notin \mathbb{L}_s$, this virtual element can not be generated by $(\mathbb{L}_d - \mathbb{L}_s) \cup (\mathbb{L}_d + \mathbb{L}_s)$. Therefore, the position $l_i + (c - a_i)(N_2 + 1)$ with $c - a_i \in [N_1, N_1 - 1 + a_{max}]$ is a hole.

$\square$

In Theorem 1, we only focus on the cross-difference set $\mathbb{L}_d - \mathbb{L}_s$ and the cross-sum set $\mathbb{L}_d + \mathbb{L}_s$. However, $(\mathbb{L}_d - \mathbb{L}_s) \cup (\mathbb{L}_d + \mathbb{L}_s)$ no longer has the hole-free property when only the remainder constraint is satisfied. There will be some holes on both sides of the consecutive segment. In order to ensure the continuity of the diff-sum coarray, the dense subarray $\mathbb{L}_d$ also requires to meet the following conditions.

Theorem 2. *If $\mathbb{L}_d$ not only satisfies the remainder constraint $\mathcal{R}[\mathbb{L}_d]_{N_2+1} = [0, N_2]$, but also meets the following continuity conditions, then the diff-sum coarray is continuous in $[-l_u, l_u]$.*

(a)   *The self-difference set $\mathbb{L}_d - \mathbb{L}_d$ can fill the holes of $(\mathbb{L}_d - \mathbb{L}_s) \cup (\mathbb{L}_d + \mathbb{L}_s)$ in the range $[0, a_{max}(N_2 + 1) - 1]$;*

(b)   *The self-sum set $\mathbb{L}_d + \mathbb{L}_d$ can fill the holes of $(\mathbb{L}_d - \mathbb{L}_s) \cup (\mathbb{L}_d + \mathbb{L}_s)$ in the range $[(2N_1 - 1)(N_2 + 1), (2N_1 - 1 + a_{max})(N_2 + 1) - 1]$;*

(c)   *The self-sum set $\mathbb{L}_d + \mathbb{L}_d$ contains the consecutive elements in the range $[(2N_1 - 1 + a_{max})(N_2 + 1), l_u]$, where $l_u > (2N_1 - 1 + a_{max})(N_2 + 1)$.*

Proof. According to Theorem 1, $(\mathbb{L}_d - \mathbb{L}_s) \cup (\mathbb{L}_d + \mathbb{L}_s)$ is continuous in the range $[a_{\max}(N_2 + 1), (2N_1 - 1)(N_2 + 1) - 1]$, and the holes exist in the range $[0, a_{\max}(N_2 + 1) - 1]$ and $[(2N_1 - 1)(N_2 + 1), (2N_1 - 1 + a_{\max})(N_2 + 1) - 1]$. If the holes can be filled by the self-difference set $\mathbb{L}_d - \mathbb{L}_d$ and the self-sum set $\mathbb{L}_d + \mathbb{L}_d$, and $\mathbb{L}_d + \mathbb{L}_d$ contains all the elements in $[(2N_1 - 1 + a_{\max})(N_2 + 1), l_u]$, then the diff-sum coarray must be continuous in the range $[0, l_u]$. Due to symmetry, we can conclude that the diff-sum coarray is continuous in the range $[-l_u, l_u]$. □

It can be seen from Theorem 2 that if the designed dense subarray $\mathbb{L}_d$ satisfies the remainder constraint and these three continuity conditions, the resulting array configuration can achieve more DOFs than TNA. At the same time, $\mathbb{L}_d$ should be as sparse as possible to reduce the mutual coupling effect.

3.2. Array Configuration

Based on the aforementioned design strategy, we propose a new nested array configuration, named the coprime transformed nested array (CTNA); its dense subarray is a coprime structure that satisfies the remainder constraint and the continuity conditions. Therefore, CTNA can effectively enhance the number of DOFs and reduce the mutual coupling effect. The sensor positions of CTNA can be given by

$$\mathbb{L}_{\text{CTNA}} = \mathbb{L}_1 \cup \mathbb{L}_2 \cup \mathbb{L}_3, \tag{20}$$

where

$$\mathbb{L}_1 = \{l(M + N) \mid 0 \leq l \leq L - 1\},$$
$$\mathbb{L}_2 = \{(L - 1)(M + N) + nM \mid 0 \leq n \leq N\},$$
$$\mathbb{L}_3 = \{(L - 1)(M + N) + mN \mid 0 \leq m \leq M\}.$$

M and N are coprime integers and we assume $2 \leq M < N$ without loss of generality. CTNA consists of three ULAs, where $\mathbb{L}_1$ is the sparse subarray and $\mathbb{L}_2 \cup \mathbb{L}_3$ is the dense subarray. As $\mathbb{L}_1, \mathbb{L}_2$ and $\mathbb{L}_3$ share the sensor located at $(L - 1)(M + N)$, the total number of sensors in CTNA is $M + N + L - 1$. It is obvious that $\mathbb{L}_2 \cup \mathbb{L}_3$ is a coprime structure with $M + N$ sensors, which has the following property.

Property 1. *The dense subarray $\mathbb{L}_2 \cup \mathbb{L}_3$ satisfies the remainder constraint, i.e., $\mathcal{R}[\mathbb{L}_2 \cup \mathbb{L}_3]_{M+N} = [0, M + N - 1]$.*

Proof. For $l_i \in \mathbb{L}_2 \cup \mathbb{L}_3$, it can be rewritten as $l_i = a_i(M + N) + b_i$, where a_i and b_i denote the quotient and remainder of $l_i/(M + N)$, $a_i \in [L - 1, L - 1 + a_{\max}]$, $b_i \in [0, M + N - 1]$, $a_{\max} = \lfloor MN/(M + N) \rfloor$. First, we need to prove that for any two elements $l_i, l_j \in \mathbb{L}_2 \cup \mathbb{L}_3$, if $l_i \neq l_j$, then remainders $b_i \neq b_j$. The proof is provided by contradiction.

When $l_i, l_j \in \mathbb{L}_2$, their remainders are $b_i = (L-1)(M+N) + n_iM - a_i(M+N)$, $b_j = (L-1)(M+N) + n_jM - a_j(M+N)$. If $b_i = b_j$, one can obtain

$$\frac{M}{N} = \frac{a_i - a_j}{n_i - n_j - a_i + a_j}. \tag{21}$$

As $a_i - a_j \in [-a_{\max}, a_{\max}]$ and $a_{\max} < \lfloor MN/N \rfloor = M$, M and N are coprime integers, and the solution of (21) is $a_i = a_j$, $n_i = n_j$, which contradicts the assumption $l_i \neq l_j$.

When $l_i, l_j \in \mathbb{L}_3$, their remainders are $b_i = (L-1)(M+N) + m_iN - a_i(M+N)$, $b_j = (L-1)(M+N) + m_jN - a_j(M+N)$. If $b_i = b_j$, one can obtain

$$\frac{M}{N} = \frac{m_i - m_j - a_i + a_j}{a_i - a_j}. \tag{22}$$

Since $a_i - a_j \in [-a_{\max}, a_{\max}]$ and $a_{\max} < \lfloor MN/2M \rfloor \leq N/2$, the solution of (22) is $a_i = a_j$, $m_i = m_j$, which contradicts $l_i \neq l_j$.

When $l_i \in \mathbb{L}_2$, $l_j \in \mathbb{L}_3$, their remainders are $b_i = (L-1)(M+N) + n_iM - a_i(M+N)$, $b_j = (L-1)(M+N) + m_jN - a_j(M+N)$. If $b_i = b_j$, then we have

$$\frac{M}{N} = \frac{m_j + a_i - a_j}{n_i - a_i + a_j}. \tag{23}$$

If $a_i > a_j$ and $a_i - a_j \in [1, a_{\max}]$, then $m_j + a_i - a_j \in [1, 2M)$ and $n_i - a_i + a_j \in (-N/2, N-1]$, and (23) has no solution due to the coprime property of M and N. If $a_i < a_j$, $a_i - a_j \in [-a_{\max}, -1]$, then $m_j + a_i - a_j \in (-M, M-1]$, $n_i - a_i + a_j \in [1, 3N/2)$, and (23) has no solution. If $a_i = a_j$, it has two solutions $n_i = 0$, $m_j = 0$ and $n_i = N$, $m_j = M$, which contradict the assumption $l_i \neq l_j$.

Therefore, the remainders of the $M + N$ elements in $\mathbb{L}_2 \cup \mathbb{L}_3$ are different from each other. As remainder $b_i \in [0, M+N-1]$, it is clear that $\mathcal{R}[\mathbb{L}_2 \cup \mathbb{L}_3]_{M+N} = \{b_1, b_2, ..., b_{M+N}\} = [0, M+N-1]$. $\square$

Since $\mathbb{L}_2 \cup \mathbb{L}_3$ satisfies the remainder constraint, the cross-difference set $\mathbb{L}_2 \cup \mathbb{L}_3 - \mathbb{L}_1$ and the cross-sum set $\mathbb{L}_2 \cup \mathbb{L}_3 + \mathbb{L}_1$ can generate a long consecutive segment. In Figure 3a, we given an example of CTNA with parameters $L = 4$, $M = 3$, $N = 4$. It is clearly seen that the dense subarray $\mathbb{L}_2 \cup \mathbb{L}_3 = \{21, 24, 25, 27, 29, 30, 33\}$ satisfies $\mathcal{R}[\mathbb{L}_2 \cup \mathbb{L}_3]_7 = [0, 6]$. Therefore, the cross sets $(\mathbb{L}_2 \cup \mathbb{L}_3 - \mathbb{L}_1) \cup (\mathbb{L}_2 \cup \mathbb{L}_3 + \mathbb{L}_1)$, as shown in Figure 3b, contain all virtual elements in the range $[6, 48]$. The holes on the left and right sides of this consecutive segment are located at $\{1, 2, 5\}$ and $\{49, 52, 53, 55\}$, respectively, which is consistent with the conclusion of Theorem 1. Based on Theorem 2, the following property holds for CTNA.
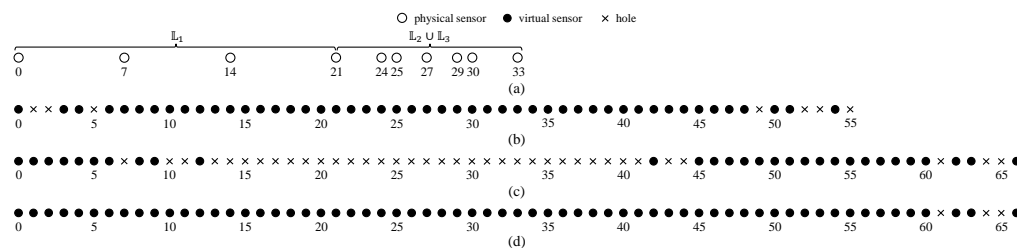

Figure 3. An example of the coprime transformed nested array and its coarrays, where $L = 4$, $M = 3$, $N = 4$. (**a**) Physical array. (**b**) Cross sets $(\mathbb{L}_2 \cup \mathbb{L}_3 - \mathbb{L}_1) \cup (\mathbb{L}_2 \cup \mathbb{L}_3 + \mathbb{L}_1)$. (**c**) Self sets $(\mathbb{L}_2 \cup \mathbb{L}_3 - \mathbb{L}_2 \cup \mathbb{L}_3) \cup (\mathbb{L}_2 \cup \mathbb{L}_3 + \mathbb{L}_2 \cup \mathbb{L}_3)$. (**d**) Diff-sum coarray.

Property 2. *The diff-sum coarray of CTNA is continuous in the range $[-l_u, l_u]$, where $l_u = 2(L-1)(M+N) + MN + M + N - 1$.*

Proof. The proof is provided in Appendix A. $\square$

An illustrative example of the above property is given in Figure 3. It is clear that the self-difference set $\mathbb{L}_2 \cup \mathbb{L}_3 - \mathbb{L}_2 \cup \mathbb{L}_3$ and the self-sum set $\mathbb{L}_2 \cup \mathbb{L}_3 + \mathbb{L}_2 \cup \mathbb{L}_3$, as shown in Figure 3c, can fill all the holes in cross sets $(\mathbb{L}_2 \cup \mathbb{L}_3 - \mathbb{L}_1) \cup (\mathbb{L}_2 \cup \mathbb{L}_3 + \mathbb{L}_1)$, which indicates that the virtual elements in the range $[0, 55]$ can be generated. In addition, the self-sum set $\mathbb{L}_2 \cup \mathbb{L}_3 + \mathbb{L}_2 \cup \mathbb{L}_3$ provides the consecutive elements in the range $[56, 60]$. The dense subarray $\mathbb{L}_2 \cup \mathbb{L}_3$ satisfies the three continuity conditions. Therefore, the diff-sum coarray of CTNA is continuous in $[-60, 60]$, as shown in Figure 3d.

4. Properties of Coprime Transformed Nested Array

4.1. Degree of Freedom

In this paper, we utilize the VCAM algorithm to perform the DOA estimation, and only the data received by the consecutive elements in the diff-sum coarray can be used. Therefore, we define the number of DOFs as the aperture of the consecutive diff-sum coarray. It can be seen from Property 2 that for a CTNA with $R = M + N + L - 1$ sensors, the number of DOFs is $4(L-1)(M+N) + 2MN + 2M + 2N - 1$. To maximize the number of DOFs provided by CTNA, we want to find the optimal choice of parameters M, N and L. This problem can be formulated mathematically as

$$
\begin{aligned}
\max_{M,N,L} \quad & 4(L-1)(M+N) + 2MN + 2M + 2N - 1, \\
\text{subject to} \quad & R = M + N + L - 1.
\end{aligned}
\tag{24}
$$

By exploiting the Lagrange multiplier method, this optimization problem can be solved, and the optimal values of M, N and L are provided in Table 1. However, the optimal values of M, N and L are not integers for most given number of sensors R, thus M and N do not satisfy the coprime assumption. In practice, we first consider the integers adjacent to the optimal values that ensure the coprimality of M and N. After that, we can determine the desired parameters by comparing the number of DOFs for each candidate.

Table 1. The optimal choice of M, N, and L and maximum number of DOFs.

	M	N	L	Maximum Number of DOFs
Optimal values	$\frac{2}{7}R + \frac{1}{7}$	$\frac{2}{7}R + \frac{1}{7}$	$\frac{3}{7}R + \frac{5}{7}$	$\frac{8}{7}R^2 + \frac{8}{7}R - \frac{5}{7}$

In order to show the advantages of the proposed CTNA, we compare the maximum number of DOFs for seven sparse arrays in Table 2, all of which consist of R sensors. It is observed that CCA [23] and PCA [27] can only obtain up to $O(\frac{R^2}{2})$ DOFs due to the existence of holes in the diff-sum coarray. By constructing a supplementary subarray to fill the holes, SCA [31] can enhance the number of DOFs to $O(\frac{25}{36}R^2)$. TNA-1, TNA-2 [29] and TwETNA [31], enjoy $O(R^2)$ DOFs, thanks to the low redundancy nested array structure. Finally, the proposed CTNA can provide $O(\frac{8}{7}R^2)$ DOFs, which is much larger than other sparse arrays.

Table 2. DOF comparison of different sparse arrays.

	Number of Sensors	Number of DOFs	Maximum Number of DOFs
CCA	$2M + N - 1$	$4MN + 2M - 1$	$O(\frac{R^2}{2} + \frac{3}{2}R)$
PCA	$M + N - 1$	$2MN + 2M + 2N - 1$	$O(\frac{R^2}{2} + 3R)$
SCA	$2M + N - 1$	$4MN + 2M + 2\lceil M/2 \rceil (M+N) - 1$	$O(\frac{25}{36}R^2 + \frac{8}{3}R)$
TNA-1	$N_1 + N_2$	$4N_1N_2 + 4N_1 - 3$	$O(R^2 + 2R)$
TNA-2	$N_1 + N_2$	$4N_1N_2 + 4N_1 + 2N_2 - 3$	$O(R^2 + 3R)$
TwETNA	$N_1 + N_2$	$4N_1N_2 + 4N_1 + 2N_2 + 2\lceil N_2/2 \rceil - 3$	$O(R^2 + \frac{7}{2}R)$
CTNA	$M + N + L - 1$	$4(L-1)(M+N) + 2MN + 2M + 2N - 1$	$O(\frac{8}{7}R^2 + \frac{8}{7}R)$

4.2. Weight Function

Different from the existing nested arrays that suffer from severe mutual coupling, the proposed CTNA achieves more DOFs while the mutual coupling effect is at the same level as the coprime arrays. Since the mutual coupling is mainly affected by the sensor pairs with small spacing, we analyze the first $M - 1$ weight function values of CTNA as follows.

Property 3. *For CTNA, the weight function $\omega(m)$ is given by*

$$\omega(m) = 2, m \in [1, M - 1] \tag{25}$$

Proof. The proof is provided in Appendix B. □

Property 3 shows that the proposed CTNA can significantly reduce the mutual coupling effect since the number of sensor pairs with small spacing is independent of the array size. In Table 3, we list the first three weight function values $\omega(1), \omega(2)$ and $\omega(3)$ for seven sparse arrays. Since the closed-form expressions for the weight functions are very complicated, here, we only consider the case of $R \geq 19$. It is obvious that for TNA-1, TNA-2 and TwETNA, the weight function $\omega(m)$ increases with the number of sensors, which indicates that the nested configurations are sensitive to mutual coupling, especially when the array size is large. On the other hand, the weight function $\omega(m)$ of CCA, PCA and CTNA is a constant value 2, which is independent of the array size. SCA can further reduce the number of sensor pairs with small spacing to $\omega(m) \leq 2$. Therefore, the mutual coupling effect of CTNA is at the same level as CCA and PCA, which is slightly higher than that of SCA. Thus, CTNA is a promising array configuration that combines the merits of the coprime array and nested array.

Table 3. Weight function comparison of different sparse array.

	Number of Sensors	Weight Functions Values
CCA	$2M + N - 1$	$\omega(1) = \omega(2) = \omega(3) = 2$
PCA	$M + N - 1$	$\omega(1) = \omega(2) = \omega(3) = 2$
SCA	$2M + N - 1$	$\omega(1) \leq 2, \omega(2) \leq 2, \omega(3) \leq 2$
TNA-1	$N_1 + N_2$	$\omega(1) = N_2, \omega(2) = N_2 - 1, \omega(3) = N_2 - 2$
TNA-2	$N_1 + N_2$	$\omega(1) = N_2 - 2, \omega(2) = N_2 - 3, \omega(3) = N_2 - 4$
TWETNA	$N_1 + N_2$	$\omega(1) = N_2 - 4, \omega(2) = N_2 - 6, \omega(3) = N_2 - 7$
CTNA	$M + N + L - 1$	$\omega(1) = \omega(2) = \omega(3) = 2$

5. Numerical Simulations

In this section, we conduct extensive numerical simulations to investigate the DOA estimation accuracy of the considered sparse arrays in the presence of mutual coupling. The VCAM algorithm is used to detect the DOAs of a set of uniform distributed sources.

5.1. Degrees of Freedom Ratio

In the first experiment, we compare the maximum number of DOFs for the seven sparse arrays using DOF ratio, which can be defined as

$$\gamma = R^2 / l_u, \tag{26}$$

where l_u represents the maximum one-side aperture of the consecutive diff-sum coarray. The smaller γ is, the larger the number of DOFs is. The DOF ratios with the number of sensors R varying from 14 to 98 are drawn in Figure 4. It is obvious that, with the increase in R, the DOF ratios of TNA-1, TNA-2 and TwETNA approach a constant 2, while that of CTNA approaches a constant 1.7, which indicates that CTNA can achieve a larger number of DOFs.
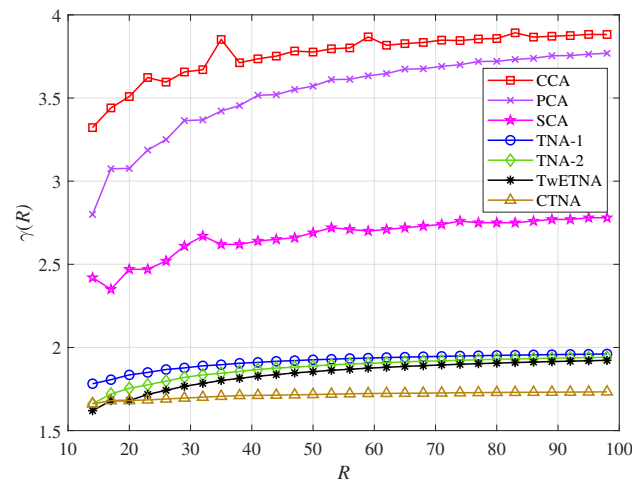
Figure 4. DOF ratio $\gamma(R)$ versus the number of sensors R.

5.2. Coupling Leakage

Then, we evaluate the mutual coupling effect of each sparse array via the coupling leakage E defined in (17). The smaller E is, the lesser the mutual coupling. Figure 5 shows the coupling leakage with the number of sensors R varying from 14 to 98, where the mutual coupling coefficient is $|c_1| = 0.3$. It is clearly seen that the coupling leakage of the proposed CTNA is at the same level as CCA and PCA, much less than TNA-1, TNA-2 and TwETNA. Therefore, CTNA is a kind of nested array that is insensitive to the mutual coupling effect.
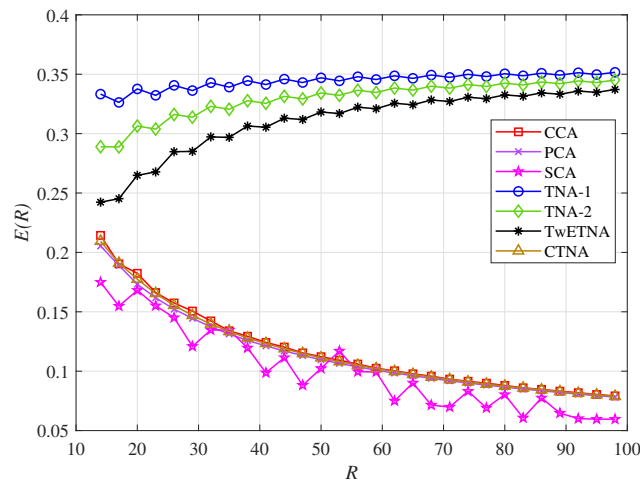

Figure 5. Coupling leakage $E(R)$ versus the number of sensors R.

5.3. DOA Estimation

In this experiment, we examine the DOA estimation performance of the 7 sparse arrays consisting of 16 sensors. The number of available DOFs, the weight function values and the coupling leakage E of these sparse arrays are provided in Table 4. $K = 41$ far-field narrowband uncorrelated sources are considered, which are uniformly distributed between $-60°$ and $60°$. The signal-to-noise ratio (SNR) is set as 0 dB, the number of snapshots T and the number of pseudo snapshots P satisfy $T = P = 800$, and the mutual coupling coefficient is $|c_1| = 0.2$.

Table 4. Character comparison for sparse arrays with $R = 16$ sensors.

	Specified Parameters	Number of DOFs	Weight Functions	E
CCA	$M = 4, N = 9$	151	$\omega(1) = \omega(2) = \omega(3) = 2$	0.1382
PCA	$M = 8, N = 9$	177	$\omega(1) = \omega(2) = \omega(3) = 2$	0.1299
SCA	$M = 5, N = 7$	221	$\omega(1) = 1, \omega(2) = 1, \omega(3) = 2$	0.1028
TNA-1	$N_1 = 8, N_2 = 8$	285	$\omega(1) = 8, \omega(2) = 7, \omega(3) = 6$	0.2306
TNA-2	$N_1 = 8, N_2 = 8$	301	$\omega(1) = 6, \omega(2) = 5, \omega(3) = 4$	0.2027
TWETNA	$N_1 = 8, N_2 = 8$	309	$\omega(1) = 4, \omega(2) = 2, \omega(3) = 3$	0.1669
CTNA	$M = 4, N = 5, L = 8$	309	$\omega(1) = \omega(2) = \omega(3) = 2$	0.1331

Figure 6 presents the normalized spatial spectra for the sparse arrays described above. Note that only CTNA can correctly identify all 41 sources due to the larger number of DOFs and lower mutual coupling. The nested array configurations TNA-1, TNA-2 and TwETNA have sufficient DOFs to detect the sources, but the severe mutual coupling effect leads to some missing sources and spurious peaks in the spatial spectra. On the other hand, the coprime array configurations CCA, PCA and SCA have a degraded spatial spectrum with missing sources due to the limitation of the number of DOFs.
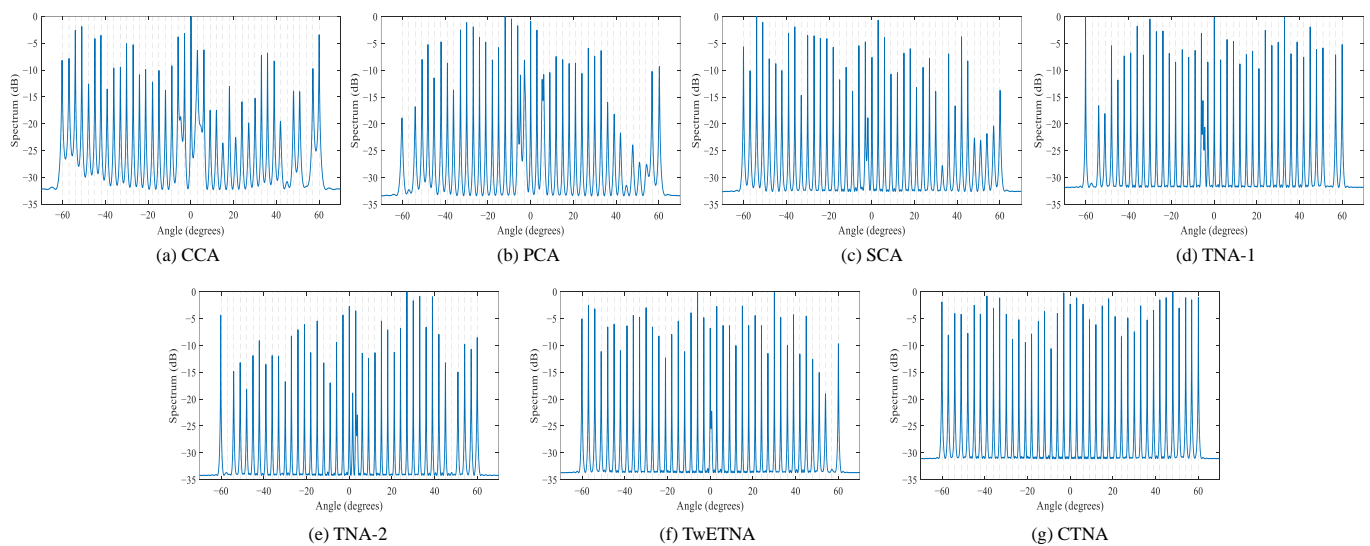

Figure 6. The VCAM spatial spectra for the considered sparse arrays with $R = 16$ sensors, where SNR = 0 dB, $T = P = 800$ and $|c_1| = 0.2$. (**a**) CCA. (**b**) PCA. (**c**) SCA. (**d**) TNA-1. (**e**)TNA-2. (**f**) TwETNA. (**g**) CTNA.

The computational time for the seven sparse arrays to perform 100 DOA estimates is shown in Table 5. The results are obtained via a personal computer with a 2.9 GHz Intel Core i7-10700 and 32 GB of RAM. It can be seen that the computational time is proportional to the maximum one-side aperture l_u, thus the proposed CTNA and TwETNA have relative higher computational complexity. However, CTNA can achieve better DOA estimation performance than TwETNA in the presence of mutual coupling.

Table 5. Computational time to perform 100 DOA estimates.

	CCA	PCA	SCA	TNA-1	TNA-2	TwETNA	CTNA
Times (s)	29.357	34.034	43.440	51.326	53.466	55.496	55.345

5.4. RMSE Results

In the last experiment, we perform 500 Monte Carlo simulations to further compare the DOA estimation accuracy through the root mean square error (RMSE), which is defined as

$$\text{RMSE} = \sqrt{\frac{1}{500K}\sum_{i=1}^{500}\sum_{k=1}^{K}(\hat{\theta}_{k,i} - \theta_k)^2}, \tag{27}$$

where $\hat{\theta}_{k,i}$ is the estimate of θ_k in the ith trial, $i = 1, 2, ..., 500$. $K = 21$ sources are distributed uniformly between $-60°$ and $60°$. The considered sparse array configurations are provided in Table 4.

Figure 7 shows the RMSE results as a function of SNR. We set the number of snapshots as $T = P = 800$ and mutual coupling coefficient as $|c_1| = 0.2$. The SNR varies from -10 dB to 20 dB. It is clearly seen that all the RMSE values decrease with the increase of SNR, and the proposed CTNA has the lowest RMSE among the seven sparse arrays due to the enhanced DOFs and reduced mutual coupling. The performance of SCA is better than other sparse arrays, but worse than CTNA, which is attributed to the sparsest array structure. Although TwETNA can provide the same number of DOFs as CTNA in this case, the high mutual coupling effect limits its performance.
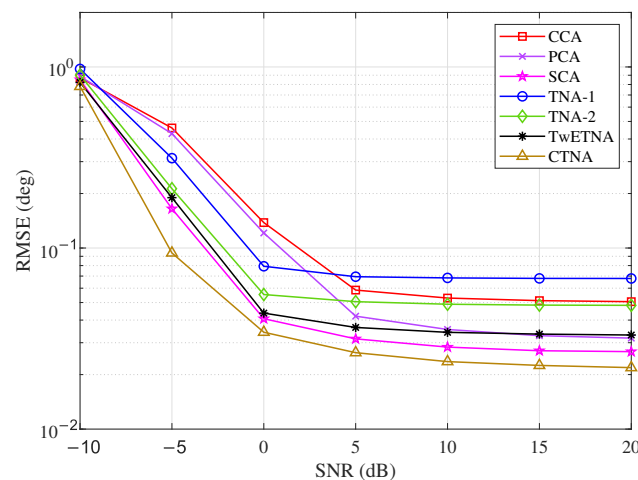

Figure 7. RMSE versus SNR, where $T = P = 800$, $|c_1| = 0.2$.

The RMSE curves versus the number of snapshots varying from 200 to 2000 are presented in Figure 8, where the fixed parameters are set to SNR = 0 dB, $|c_1| = 0.2$. It can be seen that the proposed CTNA performs better in DOA estimation than other sparse arrays, regardless of the number of snapshots. Moreover, the RMSEs of CCA and PCA suffer from deterioration until 1200 snapshots are used, while the remaining sparse arrays only need 600 snapshots to achieve satisfactory estimation accuracy, which indicates that CCA and PCA need to collect more snapshots to obtain sufficient information due to the lowest number of available DOFs.

The RMSE results versus mutual coupling coefficient $|c_1|$ are illustrated in Figure 9, where SNR=0 dB, $T = P = 800$, $|c_1|$ varies from 0 to 0.5. Similarly, CTNA achieves the best DOA estimation performance and can tolerate high levels of mutual coupling until $|c_1| = 0.4$. In comparison, the operation range of other sparse arrays is limited to $0 \le |c_1| \le 0.25$.
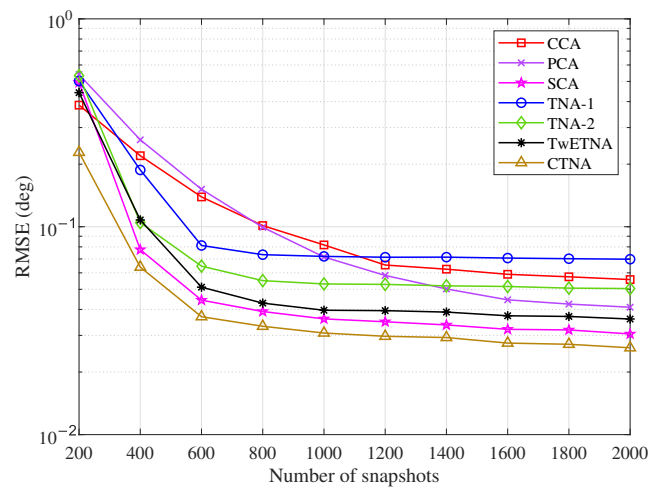
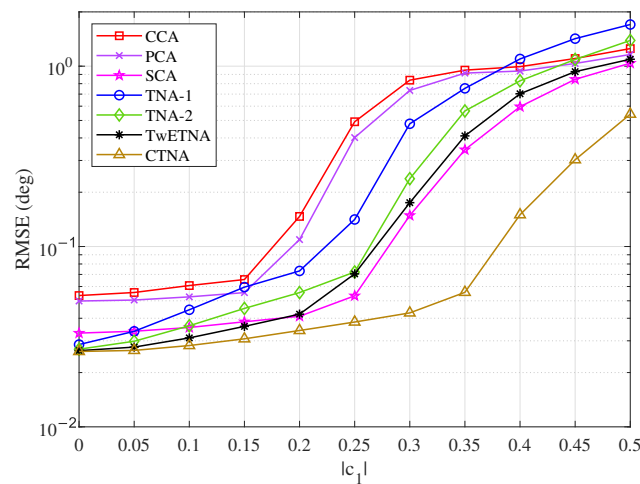**Figure 8.** RMSE versus the number of snapshots, where SNR=0 dB, $|c_1| = 0.2$.

Figure 9. RMSE versus mutual coupling coefficient $|c_1|$, where SNR = 0 dB, $T = P = 800$.

6. Conclusions

In order to expand the consecutive coarray range and reduce mutual coupling, an improved transformed nested array design strategy was proposed in this paper, which consists of the remainder constraint and three continuity conditions. Based on this strategy, we developed a novel array configuration termed coprime transformed nested array, which has the merits of both the coprime array and nested array. Specifically, CTNA can achieve a larger number of DOFs than the existing nested arrays, and the mutual coupling can be kept at a low level since its dense subarray is a coprime structure. In the end, numerical simulations were given to verify the effectiveness of the proposed CTNA in terms of the DOA estimation accuracy.

Author Contributions: Conceptualization, J.M.; data curation, J.M. and Z.P.; formal analysis, J.M. and Z.P.; funding acquisition, S.Z., W.W. and X.W.; investigation, S.Z., W.W. and X.W.; methodology, J.M.; supervision, S.Z., W.W. and X.W.; validation, J.M. and Z.P.; writing—original draft, J.M. and Z.P.; writing—review and editing, W.G. All authors have read and agreed to the published version of the manuscript.

Appendix A. Proof of Property 2

According to the property (b) of Theorem 1, the position $l_i - (a_i - c)(M + N)$ with $a_i - c \in [L, L - 1 + a_{\max}]$ is a hole in the range $[c(M + N), (c + 1)(M + N) - 1]$, where $l_i \in \mathbb{L}_2 \cup \mathbb{L}_3, c \in [0, a_{\max} - 1]$. If $l_i \in \mathbb{L}_2$, the hole position can be rewritten as

$$
\begin{aligned}
&(L - 1)(M + N) + n_i M - (a_i - c)(M + N) \\
=&[(L - 1)(M + N) + (n_i + L - 1 - a_i + c)M] - [(L - 1)(M + N) + (a_i - c - L + 1)N],
\end{aligned} \tag{A1}
$$

where $a_i - c - L + 1 \in [1, a_{\max}]$, thus $(L - 1)(M + N) + (a_i - c - L + 1)N \in \mathbb{L}_3$. As $a_i - c \geq L$, then $n_i + L - 1 - a_i + c \leq N - 1$. Meanwhile, since $(L - 1)(M + N) + n_i M \geq a_i(M + N)$, then

$$
(n_i + L - 1 - a_i)M \geq (a_i - L + 1)N \geq 0. \tag{A2}
$$

As $c \geq 0$, one can obtain $n_i + L - 1 - a_i + c \geq 0$. Therefore, $n_i + L - 1 - a_i + c \in [0, N - 1]$, $(L - 1)(M + N) + (n_i + L - 1 - a_i + c)M \in \mathbb{L}_2$, and the hole can be filled by the self-difference set $\mathbb{L}_2 \cup \mathbb{L}_3 - \mathbb{L}_2 \cup \mathbb{L}_3$. On the other hand, if $l_i \in \mathbb{L}_3$, the hole position can be rewritten as

$$
\begin{aligned}
&(L - 1)(M + N) + m_i N - (a_i - c)(M + N) \\
=&[(L - 1)(M + N) + (m_i + L - 1 - a_i + c)N] - [(L - 1)(M + N) + (a_i - c - L + 1)M].
\end{aligned} \tag{A3}
$$

Similarly, one can find that $a_i - c - L + 1 \in [1, a_{\max}]$ and $m_i + L - 1 - a_i + c \in [0, M - 1]$, thus $(L - 1)(M + N) + (a_i - c - L + 1)M \in \mathbb{L}_2$, $(L - 1)(M + N) + (m_i + L - 1 - a_i + c)N \in \mathbb{L}_3$, and the hole can be filled by the self-difference set $\mathbb{L}_2 \cup \mathbb{L}_3 - \mathbb{L}_2 \cup \mathbb{L}_3$.

According to the property (c) of Theorem 1, the position $l_i + (c - a_i)(M + N)$ with $c - a_i \in [L, L - 1 + a_{\max}]$ is a hole in the range $[c(M + N), (c + 1)(M + N) - 1]$, where $l_i \in \mathbb{L}_2 \cup \mathbb{L}_3, c \in [2L - 1, 2L - 2 + a_{\max}]$. If $l_i \in \mathbb{L}_2$, the hole position can be rewritten as

$$
\begin{aligned}
&(L - 1)(M + N) + n_i M + (c - a_i)(M + N) \\
=&[(L - 1)(M + N) + (n_i + c - a_i - L + 1)M] + [(L - 1)(M + N) + (c - a_i - L + 1)N],
\end{aligned} \tag{A4}
$$

where $c - a_i - L + 1 \in [1, a_{\max}]$, thus $(L - 1)(M + N) + (c - a_i - L + 1)N \in \mathbb{L}_3$. Since $c - a_i \geq L$, then $n_i + c - a_i - L + 1 \geq 1$. Moreover, as $(L - 1)(M + N) + n_i M < (a_i + 1)(M + N)$, then

$$
(n_i - a_i - 1)M < (a_i + 1)N - (L - 1)(M + N). \tag{A5}
$$

Adding $(c - L + 1)M$ to both sides of (A5), one can obtain

$$
(n_i + c - a_i - L)M < (a_i + 1)N + (c - L + 1)M - (L - 1)(M + N) \leq a_{\max}(M + N) < MN, \tag{A6}
$$

where the second inequality holds since $a_i + 1 \leq L - 1 + a_{\max}$ and $c - L + 1 \leq L - 1 + a_{\max}$. As a result, $n_i + c - a_i - L + 1 \leq N$, $(L - 1)(M + N) + (n_i + c - a_i - L + 1)M \in \mathbb{L}_2$, and the hole can be filled by the self-sum set $\mathbb{L}_2 \cup \mathbb{L}_3 + \mathbb{L}_2 \cup \mathbb{L}_3$. On the other hand, if $l_i \in \mathbb{L}_3$, the hole position can be rewritten as

$$
\begin{aligned}
&(L - 1)(M + N) + m_i N + (c - a_i)(M + N) \\
=&[(L - 1)(M + N) + (m_i + c - a_i - L + 1)N] + [(L - 1)(M + N) + (c - a_i - L + 1)M].
\end{aligned} \tag{A7}
$$

Similarly, $c - a_i - L + 1 \in [1, a_{\max}]$, $m_i + c - a_i - L + 1 \in [0, M]$, thus $(L - 1)(M + N) + (c - a_i - L + 1)M \in \mathbb{L}_2$, $(L - 1)(M + N) + (m_i + c - a_i - L + 1)N \in \mathbb{L}_3$, and the hole can be filled by the self-sum set $\mathbb{L}_2 \cup \mathbb{L}_3 + \mathbb{L}_2 \cup \mathbb{L}_3$.

As the dense subarray $\mathbb{L}_2 \cup \mathbb{L}_3$ is a coprime structure similar to the prototype CA, its self-sum set $\mathbb{L}_2 \cup \mathbb{L}_3 + \mathbb{L}_2 \cup \mathbb{L}_3$ is continuous in the range $[2(L - 1)(M + N) + MN - M - N + 1, 2(L - 1)(M + N) + MN + M + N - 1]$. The proof is similar to Proposition 2 of [27], and is omitted here.

We proved that $\mathbb{L}_2 \cup \mathbb{L}_3 - \mathbb{L}_2 \cup \mathbb{L}_3$ can fill the holes in $[0, a_{\max}(M+N) - 1]$, $\mathbb{L}_2 \cup \mathbb{L}_3 + \mathbb{L}_2 \cup \mathbb{L}_3$ can fill the holes in $[(2L-1)(M+N), (2L-1+a_{\max})(M+N) - 1]$, and $\mathbb{L}_2 \cup \mathbb{L}_3 + \mathbb{L}_2 \cup \mathbb{L}_3$ contains all the consecutive elements in the range $[2(L-1)(M+N) + MN - M - N + 1, 2(L-1)(M+N) + MN + M + N - 1]$. Based on Theorem 2, we can conclude that CTNA is continuous in the range $[-l_u, l_u]$, where $l_u = 2(L-1)(M+N) + MN + M + N - 1$.

Appendix B. Proof of Property 3

As the subarrays $\mathbb{L}_1$, $\mathbb{L}_2$ and $\mathbb{L}_3$ are uniform linear arrays with inter-element spacing $M+N$, M and N, respectively, the weight function $\omega(m)$ for $m \in [1, M-1]$ only depends on the interaction between $\mathbb{L}_2$ and $\mathbb{L}_3$. Suppose that two different sensor pairs $\{l_1, l_2\}$ and $\{l_3, l_4\}$ contribute to the weight function $\omega(m)$, i.e., $l_1 - l_2 = l_3 - l_4 = m$, where $m \in [1, M-1]$. We need to consider the following three cases.

(a) If $l_1, l_3 \in \mathbb{L}_2$, $l_2, l_4 \in \mathbb{L}_3$, then we have

$$n_1 M - m_1 N = n_2 M - m_2 N. \tag{A8}$$

This equation can be rewritten as

$$(n_1 - n_2)M = (m_1 - m_2)N. \tag{A9}$$

Since $n_1, n_2 \in [0, N]$, $m_1, m_2 \in [0, M]$, then $n_1 - n_2 \in [-N, N]$, $m_1 - m_2 \in [-M, M]$. As M and N are coprime integers, (A9) has three solutions: $n_1 = n_2$, $m_1 = m_2$; $n_1 = N$, $n_2 = 0$, $m_1 = M$, $m_2 = 0$; $n_1 = 0$, $n_2 = N$, $m_1 = 0$, $m_2 = M$. None of these three solutions satisfy the assumption $\{l_1, l_2\} \neq \{l_3, l_4\}$.

(b) If $l_1, l_3 \in \mathbb{L}_3$, $l_2, l_4 \in \mathbb{L}_2$, then we have

$$m_1 N - n_1 M = m_2 N - n_2 M. \tag{A10}$$

This equation can be rewritten as

$$(n_2 - n_1)M = (m_2 - m_1)N. \tag{A11}$$

Since (A11) has a similar form to (A9), it is easy to find that the solutions of (A11) do not satisfy the assumption $\{l_1, l_2\} \neq \{l_3, l_4\}$.

(c) If $l_1, l_4 \in \mathbb{L}_2$, $l_2, l_3 \in \mathbb{L}_3$, then we have

$$n_1 M - m_1 N = m_2 N - n_2 M. \tag{A12}$$

This equation can be rewritten as

$$(n_1 + n_2)M = (m_1 + m_2)N, \tag{A13}$$

where $n_1 + n_2 \in [0, 2N]$, $m_1 + m_2 \in [0, 2M]$. Only when $n_1 + n_2 = N$ and $m_1 + m_2 = M$, (A13) holds and satisfies the assumption $\{l_1, l_2\} \neq \{l_3, l_4\}$.

From the above discussion, it is clear that only two sensor pairs, i.e., $\{(L-1)(M+N) + n_1 M, (L-1)(M+N) + m_1 N\}$ and $\{(L-1)(M+N) + (M-m_1)N, (L-1)(M+N) + (N-n_1)M\}$, contribute the weight function $\omega(m)$. Therefore, we can conclude that $\omega(m) = 2$ for $m \in [1, M]$.

References

1. Krim, H.; Viberg, M. Two decades of array signal processing research: The parametric approach. *IEEE Signal Process. Mag.* **1996**, *13*, 67–94. [CrossRef]
2. Qin, S.; Zhang, Y.D.; Amin, M.G. DOA estimation of mixed coherent and uncorrelated targets exploiting coprime MIMO radar. *Digit. Signal Process.* **2017**, *61*, 26–34. [CrossRef]
3. Zhang, Q.; Huang, J. Joint estimation of DOA and time-delay in underwater localization. In Proceedings of the 1999 IEEE International Conference on Acoustics, Speech, and Signal Processing. Proceedings. ICASSP99 (Cat. No.99CH36258), Phoenix, AZ, USA, 15–19 March 1999; Volume 5, pp. 2817–2820. [CrossRef]

4. Vijayan, D.M.; Menon, S.K. Direction of arrival estimation in smart antenna for marine communication. In Proceedings of the 2016 International Conference on Communication and Signal Processing (ICCSP), Melmaruvathur, India, 6–8 April 2016; pp. 1535–1540. [CrossRef]

5. Bailleul, P.K. A new era in elemental digital beamforming for spaceborne communications phased arrays. *Proc. IEEE* **2016**, *104*, 623–632. [CrossRef]

6. Amin, M.G.; Wang, X.; Zhang, Y.D.; Ahmad, F.; Aboutanios, E. Sparse arrays and sampling for Interference mitigation and DOA estimation in GNSS. *Proc. IEEE* **2016**, *104*, 1302–1317. [CrossRef]

7. Zheng, H.; Shi, Z.; Zhou, C.; Haardt, M.; Chen, J. Coupled Coarray Tensor CPD for DOA Estimation with Coprime L-Shaped Array. *IEEE Signal Process. Lett.* **2021**, *28*, 1545–1549. [CrossRef]

8. Zhou, C.; Gu, Y.; He, S.; Shi, Z. A Robust and Efficient Algorithm for Coprime Array Adaptive Beamforming. *IEEE Tran. Veh. Technol.* **2018**, *67*, 1099–1112. [CrossRef]

9. Schmidt, R. Multiple emitter location and signal parameter estimation. *IEEE Trans. Antennas Propag.* **1986**, *34*, 276–280. [CrossRef]

10. Roy, R.; Kailath, T. ESPRIT-estimation of signal parameters via rotational invariance techniques. *IEEE Trans. Acoust. Speech Signal Process.* **1989**, *37*, 984–995. [CrossRef]

11. Moffet, A. Minimum-redundancy linear arrays. *IEEE Trans. Antennas Propag.* **1968**, *16*, 172–175. [CrossRef]

12. Bloom, G.; Golomb, S. Applications of numbered undirected graphs. *Proc. IEEE* **1977**, *65*, 562–570. [CrossRef]

13. Pal, P.; Vaidyanathan, P.P. Nested arrays: A novel approach to array processing with enhanced degrees of freedom. *IEEE Trans. Signal Process.* **2010**, *58*, 4167–4181. [CrossRef]

14. Liu, C.; Vaidyanathan, P.P. Super nested arrays: Linear sparse arrays with reduced mutual coupling—Part I: Fundamentals. *IEEE Trans. Signal Process.* **2016**, *64*, 3997–4012. [CrossRef]

15. Liu, C.; Vaidyanathan, P.P. Super nested arrays: Linear sparse arays with reduced mutual coupling—Part II: High-order extensions. *IEEE Trans. Signal Process.* **2016**, *64*, 4203–4217. [CrossRef]

16. Liu, J.; Zhang, Y.; Lu, Y.; Ren, S.; Cao, S. Augmented nested arrays with enhanced DOF and reduced mutual coupling. *IEEE Trans. Signal Process.* **2017**, *65*, 5549–5563. [CrossRef]

17. Ren, S.; Dong, W.; Li, X.; Wang, W.; Li, X. Extended nested arrays for consecutive virtual aperture enhancement. *IEEE Signal Process. Lett.* **2020**, *27*, 575–579. [CrossRef]

18. Vaidyanathan, P.P.; Pal, P. Sparse sensing with co-prime samplers and arrays. *IEEE Trans. Signal Process.* **2011**, *59*, 573–586. [CrossRef]

19. Zhou, C.; Gu, Y.; Shi, Z.; Zhang, Y.D. Off-Grid Direction-of-Arrival Estimation Using Coprime Array Interpolation. *IEEE Signal Process. Lett.* **2018**, *25*, 1710–1714. [CrossRef]

20. Zhou, C.; Gu, Y.; Fan, X.; Shi, Z.; Mao, G.; Zhang, Y.D. Direction-of-Arrival Estimation for Coprime Array via Virtual Array Interpolation. *IEEE Trans. Signal Process.* **2018**, *66*, 5956–5971. [CrossRef]

21. Liu, C.; Vaidyanathan, P.P. Remarks on the spatial smoothing step in coarray MUSIC. *IEEE Signal Process. Lett.* **2015**, *22*, 1438–1442. [CrossRef]

22. Stoica, P.; Nehorai, A. MUSIC, maximum likelihood, and Cramer-Rao bound. *IEEE Trans. Acoust. Speech Signal Process.* **1989**, *37*, 720–741. [CrossRef]

23. Pal, P.; Vaidyanathan, P.P. Coprime sampling and the music algorithm. In Proceedings of the 2011 Digital Signal Processing and Signal Processing Education Meeting (DSP/SPE), Sedona, AZ, USA, 4–7 January 2011; pp. 289–294. [CrossRef]

24. Raza, A.; Liu, W.; Shen, Q. Thinned coprime array for second-order difference co-array generation with reduced mutual coupling. *IEEE Trans. Signal Process.* **2019**, *67*, 2052–2065. [CrossRef]

25. Zheng, W.; Zhang, X.; Wang, Y.; Shen, J.; Champagne, B. Padded coprime arrays for improved DOA estimation: Exploiting hole representation and filling strategies. *IEEE Trans. Signal Process.* **2020**, *68*, 4597–4611. [CrossRef]

26. Fu, Z.; Chargé, P.; Wang, Y. Rearranged coprime array to increase degrees of freedom and reduce mutual coupling. *Signal Process.* **2021**, *183*, 108038. [CrossRef]

27. Wang, X.; Chen, Z.; Ren, S.; Cao, S. DOA estimation based on the difference and sum coarray for coprime arrays. *Digit. Signal Process.* **2017**, *69*, 22–31. [CrossRef]

28. Chen, Z.; Ding, Y.; Ren, S.; Chen, Z. A novel nested configuration based on the difference and sum co-array concept. *Sensors* **2018**, *18*, 2988. [CrossRef]

29. Wang, Y.; Wu, W.; Zhang, X.; Zheng, W. Transformed nested array designed for DOA estimation of non-circular signals: Reduced sum-difference co-array redundancy perspective. *IEEE Commun. Lett.* **2020**, *24*, 1262–1265. [CrossRef]

30. Peng, Z.; Ding, Y.; Ren, S.; Wang, X. Extended transformed nested arrays for DOA estimation of non-circular sources. *IEEE Access* **2020**, *8*, 162350–162362. [CrossRef]

31. Peng, Z.; Ding, Y.; Ren, S.; Wang, W.; Gu, W. Supplementary coprime array with enhanced DOFs exploiting hole filling strategy based on the difference and sum coarray. *Digit. Signal Process.* **2022**, *121*, 103325. [CrossRef]

32. Friedlander, B.; Weiss, A.J. Direction finding in the presence of mutual coupling. *IEEE Trans. Antennas Propag.* **1991**, *39*, 273–284. [CrossRef]

33. Svantesson, T. Mutual coupling compensation using subspace fitting. In Proceedings of the 2000 IEEE Sensor Array and Multichannel Signal Processing Workshop. SAM 2000 (Cat. No.00EX410), Cambridge, MA, USA, 17 March 2000; pp. 494–498. [CrossRef]
34. Liao, B.; Zhang, Z.; Chan, S. DOA estimation and tracking of ULAs with mutual coupling. *IEEE Trans. Aerosp. Electron. Syst.* **2012**, *48*, 891–905. [CrossRef]